10 Methionine to Leucine Mutation of the Ligand to the Primary Electron Acceptor A_0

Thus far, the question of electron transfer along one or both branches of cofactors in PS I has been studied by engineering PsaA and PsaB specific mutants around the respective A_1 binding sites. Much of the published work and studies described in Chapters 8 and 9 concerning this topic focuse on these mutations because charge separation has already taken place and the electron transfer pathway is presumed to have been decided by this point. However, changes in the A_1 site lead to only subtle differences in the properties of the quinones, and their proximity to F_X, which is common to both branches. Next we therefore decided to focus on constructing mutations at the A_0 site upstream from A_1 in the electron transfer chain. These mutations should enable us to influence the properties of A_0, which we expect to affect both the quantum yield and the kinetics of electron transfer along the two branches. One complication arising from mutations is that they may influence the initial charge separation and thereby force electron transfer along an otherwise inactive pathway. Indeed, preliminary evidence to this effect has been presented in a congress report for A_0 mutants of the PsaA side of *Chlamydomonas reinhardtii* [103]. However, by constructing identical mutations on either the PsaA-side or the PsaB-side, we expect any asymmetry in the electron transfer pathway to be reflected in the phenotypes, *i.e.* if the electron transfer uses both branches we should obtain similar phenotypes for the two mutants, while asymmetric electron transfer using primarily one branch would lead to very different phenotypes.

To influence the properties of A_0, it is particularly attractive to make point mutations of the methionine residues $M688_{PsaA}$ and $M668_{PsaB}$ that provide the axial ligands to the respective Mg^{2+} ions of the two chlorophylls [1, 4]. We expect that a change in these ligands will likely alter the midpoint potential of the A_0^-/A_0 redox pair. This should result

in a change in Gibbs free energy associated with both the forward and back electron transfer from A_0^- due to a change in the Frank-Condon factor in the Marcus equation, which relates the rate of electron transfer to changes in Gibbs free energy and reorganization energy [104]. This should have several consequences. First, it may have a significant effect on the temperature dependence of the rates, since the activation energy for forward electron transfer from A_0 to A_1 is known to be small in native PS I. Second, depending on how the midpoint potential is affected a recombination of $P_{700}^+A_0^-$ to the $^3P_{700}$ triplet state may be able to compete with the forward electron transfer. Consequently, the quantum yield of charge separation beyond A_0 may be reduced and the spin polarization patterns of the subsequent radical pairs $P_{700}^+A_1^-$ and $P_{700}^+F_X^-$ may be altered.

Here, a spectroscopic characterization of the methionine to leucine point mutants of the putative A_0 binding sites in the PsaA and PsaB proteins of *Synechocystis* sp. PCC 6803 will be reported. It will be shown that the mutation in the PsaA protein has a pronounced effect on the spectroscopic properties of the PS I complex while the corresponding mutation in PsaB protein has almost no effect. This result clearly suggests a strong asymmetry in the electron transfer pathway in cyanobacterial PS I.

10.1 Transient EPR characterisation of $P_{700}^+A_1^-$ radical pair at X- and Q-Band:

10.1.1 Efficiency of Electron Transfer at Low Temperature

Several independent methods have been used for the determination of electron transfer efficiency at room and low temperatures. For example, single turnover flash excitation of PS I complexes with the measurements of ? A at 820 nm can be used to characterize the relative quantum yield of charge separation in the WT and the mutants. This method demonstrated a reduction in the overall quantum yield of charge separation in the PsaA-side mutant but not in the PsaB-side mutant as compared with the WT, for details

see [105] . This could be due to differences in the efficiency either of the excitation energy transfer to P_{700} or of the electron transfer from P_{700} to the iron-sulphur clusters. The kinetics of the absorbance change and the decay-associated spectra in the visible region provide additional information, and allow these two possibilities to be distinguished [106]. The general observation was that with respect to the kinetics of the absorbance changes the two mutants differ significantly from each other and both from the wild type. Together, the initial amplitudes, kinetics and saturation behavior of the absorbance changes suggest that the PsaA-side mutation results in a lower yield of charge separation between P_{700} and the iron-sulphur clusters compared to the wild type. It can be proposed that in the majority of PS I complexes, the electron is not transferred beyond A_0^-. In these instances, $^3P_{700}$ is populated with a low quantum yield at room temperature, leading to charge recombination between P_{700}^+ and A_0^- directly to the ground state, see scheme 10.1. The PsaB-side mutation on the other hand shows only a change in the backreaction kinetics but the overall efficiency of energy and electron transfer P_{700} and the iron-sulphur clusters is similar to the wild-type, for more details see [105].

Another way of estimating the efficiency of the charge separation in the mutants is to measure the amplitude of the spin polarized EPR spectrum of $P_{700}^+A_1^-$ generated by flash excitation. Compared to CW-EPR, time-resolved EPR has the advantage that the light-induced paramagnetic states are observed during a single turnover of the reaction center rather than as a steady-state population. Moreover, the spin polarization provides additional structural and dynamic information (for a review see [33]). In Figure 10.1, X-band (top) and Q-band (bottom) spin polarization patterns of $P_{700}^+A_1^-$ at 80K are compared for the wild-type, $M688L_{PsaA}$ and $M668L_{PsaB}$ mutants. The observed patterns are quite similar and differ mostly in their relative amplitudes. It is important to note that care was taken to ensure identical experimental conditions with respect to microwave power, laser

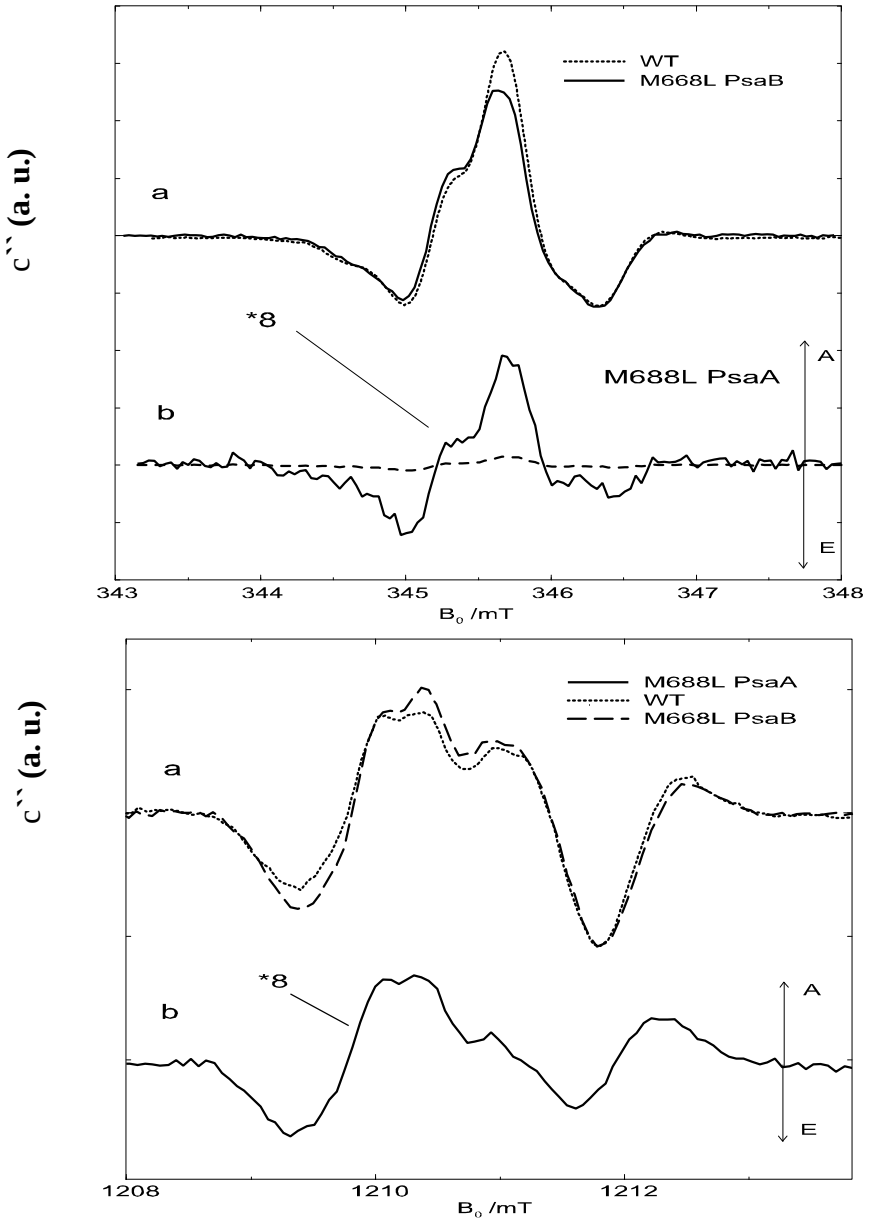

Figure 10.1 Transient spin polarised EPR spectra of the wild-type, M688L$_{PsaA}$ and M668L$_{PsaB}$ mutants at 80K. Top: X-band transient spin polarised EPR spectra due to the $P_{700}^{+}A_1^{-}$ radical pair state, as also observed in the center of the spectra of Figure 10.2. They are presented here in an expanded magnetic field range (5mT). a: comparison of very similar patterns for wild type (WT) and the M668L$_{PsaB}$ mutant (digital time integration window of 0.25-1.4 μs; microwave power 1.8 mW). b: corresponding $P_{700}^{+}A_1^{-}$ spectra of M688L$_{PsaA}$ mutant, recorded under the same instrumental conditions as used for upper spectra (dashed line) and amplified by a factor 8 (solid line). Bottom: Q-band spectra of the same set of samples. a: comparison of wild type (WT) with the M668L$_{PsaB}$ mutant b: M688L$_{PsaA}$ pattern, amplified by a factor of 8 compared to the instrumental settings for the top spectra.

intensity, cavity setting, sample concentration and other relevant instrumental parameters so that the relative signal intensities reflect differences in the quantum yield of $P_{700}^{+}A_1^{-}$ and its spin polarization. The spectral patterns of the wild-type and the M668L_{PsaB} mutant do not show any significant differences either at the X-band or the Q-band (Figure 10.1 a). In contrast, the polarization pattern from the M688L_{PsaA} mutant is changed significantly and the relative signal amplitude is reduced by nearly an order of magnitude compared to that of the wild-type and the M668L_{PsaB} mutant (Figure 10.1 b). We can rule out the possibility that this change in amplitude is due to weaker spin polarization. Hence, the weaker signal intensity can be attributed to a lower quantum yield of $P_{700}^{+}A_1^{-}$ formation.

10.1.2 Spin polarisation patterns of $P_{700}^{+}A_1^{-}$

The spectral patterns of the wild-type and the M668L_{PsaB} mutant do not show any significant differences at either X-band or Q-band (Figure 10.1a). In contrast, the polarization pattern from the M688L_{PsaA} mutant is changed significantly. The Q-band spectra shown in Figure 10.1 (bottom) confirm that the quinone orientation is not significantly altered in the mutants. The higher microwave frequency and magnetic field at the Q-band lead to higher *g*-tensor resolution and better separation of the contributions from P_{700}^{+} and A_1^{-} to the polarization patterns. The pattern from the PsaA-side mutant in Figure 10.1b (bottom) shows significant differences, between PsaA mutant and WT, however restricted to the region dominated by contributions from P_{700}^{+}. As can be seen in Figure 10.1b (bottom), the relative amplitude of the predominantly emissive feature on the up-field side of the pattern from the PsaA-branch mutant is considerably weaker than in the spectrum of the wild-type. Except for the overall amplitude reduction, the changes in the region dominated by the quinone (left half of the pattern) are minimal.

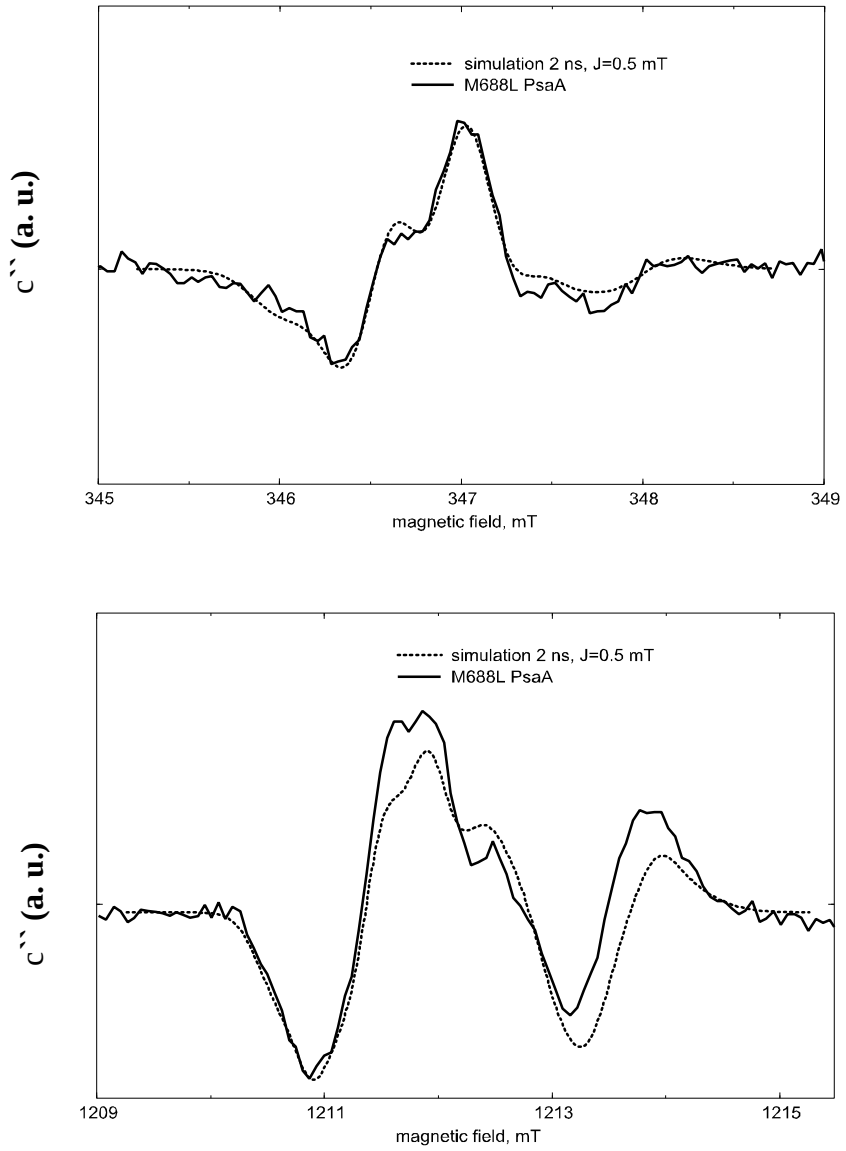

Figure 10.2 Comparison of experimental (solid) and simulated (dotted line) patterns at the X-band (top) and Q-band (bottom) spectrum of the $P_{700}^{+}A_1^{-}$ state in PS I of the $M688L_{PsaA}$ mutant. The most favorable comparison is obtained with the following simulation parameters for the precursor pair state $P_{700}^{+}A_0^{-}$: exchange integral J = 0.5 mT and lifetime τ = 2 ns.

The change of the $P_{700}^{+}A_1^{-}$ EPR spectrum of $M688L_{PsaA}$ compared to the wild type reaction center spectrum can be interpreted as a result of an increased lifetime of the electron in the precursor pair $P_{700}^{+}A_0^{-}$ state (Scheme 10.1). By comparison of experimental (see Figure 10.2) with simulated spectra the experimental polarisation patterns for the $M688L_{PsaA}$ mutant (solid line) are simulated satisfactorily with a lifetime of the $P_{700}^{+}A_0^{-}$ state around 2 ns and an exchange integral around 0.5 mT (for details of spectra simulations see [107]). The character of the observed change requires that the exchange interaction in the $P_{700}^{+}A_0^{-}$ state is positive (ferromagnetic).

Scheme 10.1: Electron transfer and spin dynamics in the $M688L_{PsaA}$ mutant

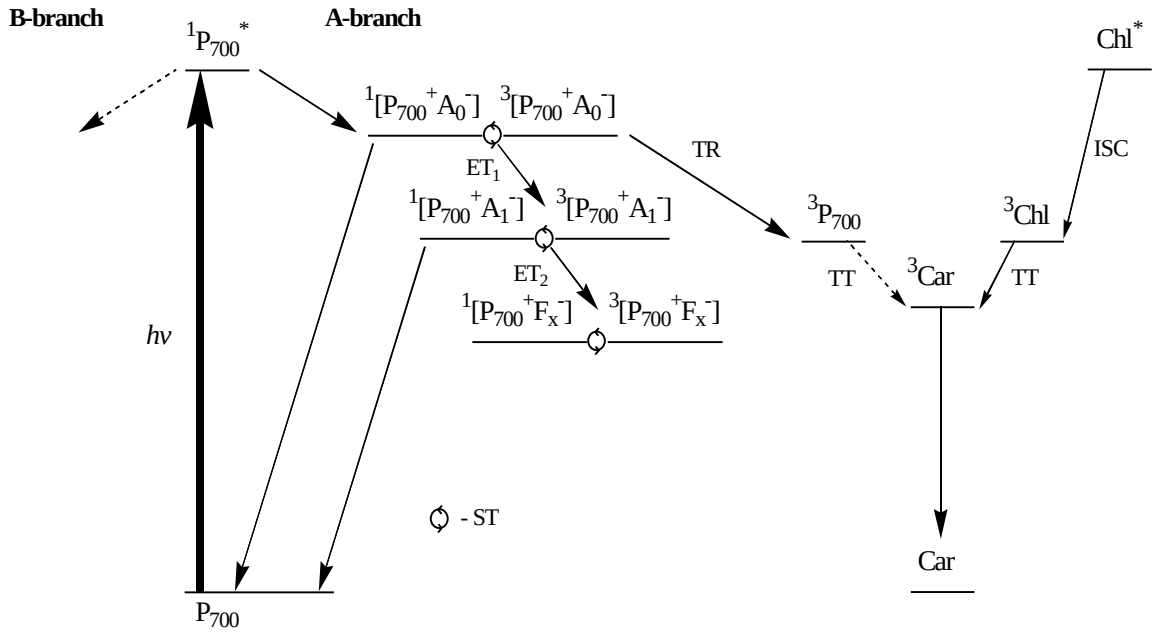

TR: triplet radical pair recombination with characteristic spin polarisation due to $\Delta m=0$ selection.
TT: triplet state transfer or trapping
ISC: intersystem crossing with zero-field spin selectivity
CS: primary charge separation
ET: spin conserving electron transfer
ET_1: primary electron transfer from A_0 to A_1
ET_2: secondary electron transfer from A_1 to the iron-sulphur centers, time constant 290 ns at room temperature
ST: singlet-triplet mixing in the radical pair state, typical time constant: ≈0.5 ns.

10.2 Observation of $^3P_{700}$ due to Charge Recombination by Time-Resolved EPR Spectroscopy

The difference between the spectra of the M688L_{PsaA} and M668L_{PsaB}/WT in Figure 10.1 is the reduced relative amplitude of the spectrum from the PsaA-side mutant, which suggests a much lower yield of reversible $P_{700}^+A_1^-$ formation. If this results from an increased yield of charge recombination from $P_{700}^+A_0^-$ for the PsaA-side mutant then population of the triplet state of P_{700} is predicted, which should be observable by transient EPR.

Figure 10.3 (Top) shows a comparison of X-band transient EPR spectra taken under the same conditions as those in Figure 10.1 but over a wider field range to confirm the presence or absence of triplet states. The spectra of the wild-type and the M668L_{PsaB} mutant (Figure 10.3, top) show a common weak background signal and only the signal from $P_{700}^+A_1^-$ is seen as narrow spikes in the center of the spectral range. In contrast, the M688L_{PsaA} mutant has a sizeable contribution from the broad spectrum of $^3P_{700}$. The observed polarization pattern is unique to triplet states formed by radical pair recombination and is incompatible with other pathways such as intersystem crossing (ISC) because charge recombination is the only process which can lead to exclusive population of the T_0 spin level. Thus, the polarization pattern serves as a fingerprint for $^3P_{700}$ formation by recombination from $P_{700}^+A_0^-$, for a review see [108]. The reduction in the amplitude of the $P_{700}^+A_1^-$ radical pair spectrum (Figure 10.1) correlates with the appearance $^3P_{700}$ spectrum due to charge recombination, which indicates that forward electron transfer past A_0 is severely impaired in the PsaA-side mutant.

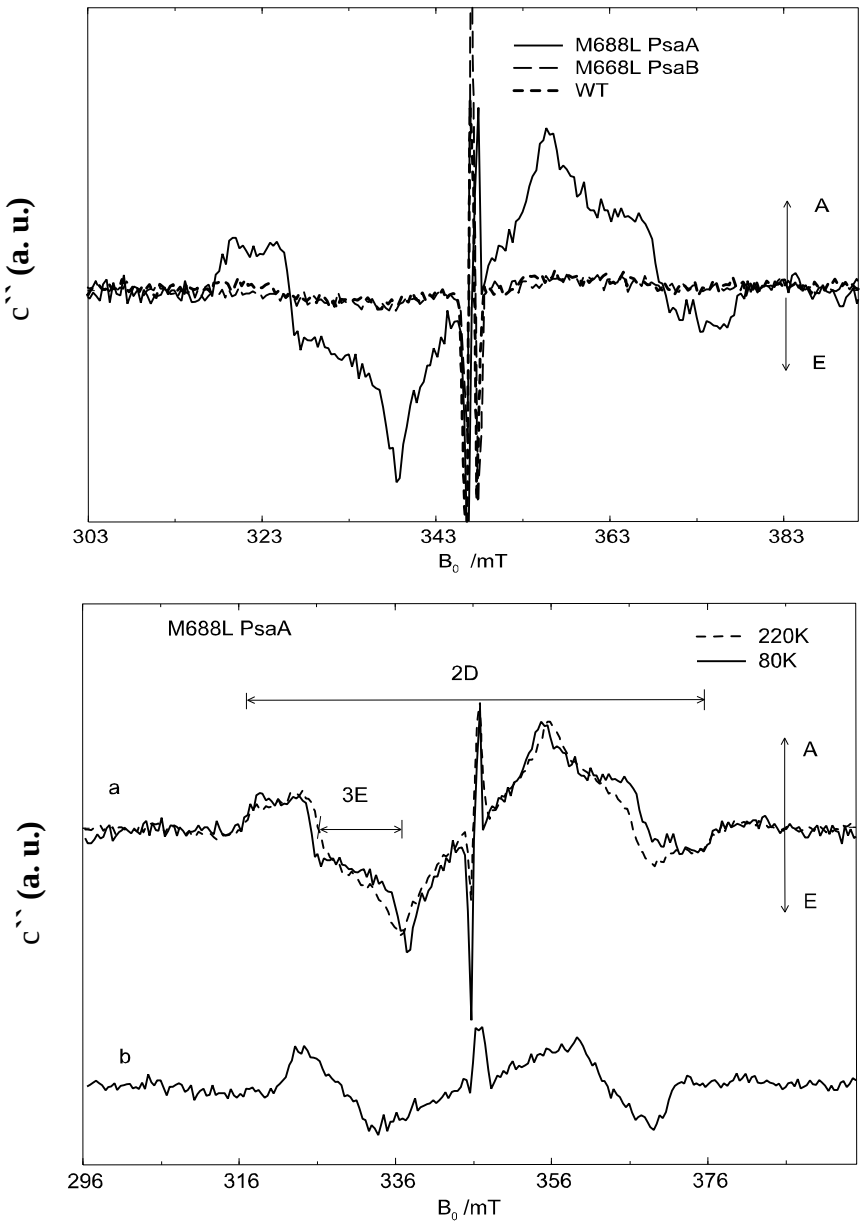

Figure 10.3 Top: spin polarised transient EPR spectra at 80K and X-band for wide field scan (100 mT) for wild type (WT) (dotted line) and the mutants M688L$_{PsaA}$ (solid line), M668L$_{PsaB}$ (broken line). The spectra are extracted from complete time/field scans in an early digital time integration window of 0.25-1.4 μs (field steps of 0.4 mT, microwave power 7 mW). Positive amplitude corresponds to absorptive (A) and negative to emissive (E) EPR signal. Bottom: a) comparison of X-band TR-EPR $^3P_{700}$ triplet spectra of the M688L$_{PsaA}$ mutant at two temperatures: 80 K and 220 K. Magnetic field sweep, field steps and other experimental conditions as in the top Figure. The zero field splitting parameters $|D|$ and $|E|$ are indicated as derived from the high field approximation. b) Late triplet spectrum observed in the M688L$_{PsaA}$ mutant, 80K, time integration window 4-15 μs. The signal is assigned to ^{3}Car populated via intersystem crossing-populated ^{3}Chl (see text).

The significance of this result is that it not only confirms that at low temperature reversible electron transfer occurs in the PsaA- branch of co-factors, but it also shows that when this pathway is blocked electrons are not re-routed along the PsaB-branch.

The saturation behavior and kinetics of the optical absorbance changes suggest that at high light intensities, carotenoid triplet states are also formed in the antenna. This is consistent with the EPR data, which show a characteristic longer-lived triplet spectrum at late times after decay of the $^3P_{700}$ spectrum (Figure 10.3b, bottom). Similar spectra have been reported previously for purple bacteria [109] and PS II [110]. They are attributed to a long-lived carotenoid triplet state populated by triplet-triplet energy transfer from a chlorophyll triplet with characteristic spin polarisation associated with an intersystem crossing population process. In these systems, excitation energy that cannot be trapped by the reaction center eventually leads to population of ^{3}Chl in the antenna via intersystem crossing. This triplet state is then efficiently quenched by a triplet exchange mechanism to ^{3}Car (as observed optically [111] or by EPR [109, 110]). In PS I, 60 of the 90 antenna chlorophylls are in direct van der Waals contact to carotenoids [1, 4] which are known to act as triplet quenchers. Hence we conclude that the A-side mutation may also reduce the efficiency of excitation energy transfer to the reaction center, in addition to reducing the quantum yield of charge separation to A_1.

10.3 Influence of Met to Leu Mutation in the A_0 Binding Site on the Electron Transfer in Photosystem I.

In order to study PS I electron transfer at a primary level and to better understand interactions between the protein and the chlorophyll molecules involved, the methionines that provide the axial ligands to the Mg^{2+} ions of the chlorophylls that putatively function

as A_0 were mutated for either the A-side or the B-side of the quasi symmetric PS I heterodimer. For this the methionine residue was replaced by a leucine residue at position $M688_{PsaA}$ and $M668_{PsaB}$, respectively. A profound alternation in PS I forward electron transfer was observed for the A-side mutant only, while the TR-EPR spectra remained indistinguishable for the B-side mutant and the wild type. Thus, these mutants can be useful for an investigation of the directionality of electron transfer in PS I. The most striking EPR result is the appearance of a $^3P_{700}$ signal contribution with the characteristic spin polarisation pattern due to radical pair recombination in the T_0 state, but only for the $M688L_{PsaA}$ mutant. The triplet contribution is readily detectable from low temperature (below 80K) up to at least 260K (Figure 10.3). Evidence exists that it is populated also at higher temperatures but the combination of decreasing triplet yield and faster signal decay, due to faster spin relaxation with increasing temperature, degrade EPR-detectability rapidly. In general, the appearance of a $^3P_{700}$ signal contribution is combined with a reduction in yield of forward electron transfer to the TR-EPR detected $P_{700}^+A_1^-$ charge-separated state. Again, this is observed for the A-side mutant only.

It should be noted that at low temperature (e.g. 80 K) the rise time of the $^3P_{700}$ signal is measured to be about 200 ns, in any case definitely slower than the instrumental rise time (about 50 ns). This value is in agreement with the optical data obtained earlier for the triplet rise time at lower temperature [112]. In addition, the forward electron transfer from A_0 to A_1 is evaluated to be in the range of 2 ns from the observed spin polarisation pattern of the $P_{700}^+A_1^-$ state. Therefore it is slowed down by at least an order of magnitude compared to WT PS I (30 – 50 ps) in PsaA mutant only. However, a major difference remains between the rise times of the $^3P_{700}$ and $P_{700}^+A_1^-$ signal contribution. This is not compatible with a branching at the $P_{700}^+A_0^-$ level because it would correspond to only a

minor triplet signal. The result would be consistent with different fractions of PS I centers associated with each of the signal contributions.

Here the fact of a slow (ca. 200 ns) $^3P_{700}$ signal rise time at low temperature is significant because by comparison, a detectable triplet contribution should also be observed for the PsaB side mutant, if a significant portion of electron transfer proceeds along this branch. Indeed, the assignment of the "fast optical phase" in the A_1 reoxidation kinetics to B-branch electron transfer requires about 1/3 of electron transfer activity along the B-branch. This would result in an observable $^3P_{700}$ signal contribution for the PsaB-side mutant provided the structural homology between the two A_0 sites has the consequence that a mutation of the methionine axial ligand to A_0 has essentially the same effects on the electron transfer properties in both branches. In this respect the fact that no $^3P_{700}$ signal contribution is observed for the PsaB-side mutant is evidence against significant electron transfer activity along the B-branch.

In summary, all data presented here are consistent with highly asymmetrical electron transfer along the PsaA-branch of cyanobacterial PS I. We intend to supplement the data with picosecond optical kinetic data for the primary charge separation events with the hope to measure the lifetime of the $P_{700}^+A_0^-$ radical pair state directly and confirm the values concluded here from simulation of the EPR polarization patterns.